



# Light-induced interconnects using nonlinear Airy beam interactions

Thomas Bouchet, Nicolas Marsal, Marc Sciamanna, D. Wolfersberger

## ► To cite this version:

Thomas Bouchet, Nicolas Marsal, Marc Sciamanna, D. Wolfersberger. Light-induced interconnects using nonlinear Airy beam interactions. *Journal of Physics: Photonics*, 2019, 1 (2), pp.025001. 10.1088/2515-7647. hal-01988735

**HAL Id: hal-01988735**

**<https://centralesupelec.hal.science/hal-01988735>**

Submitted on 1 Dec 2020

**HAL** is a multi-disciplinary open access archive for the deposit and dissemination of scientific research documents, whether they are published or not. The documents may come from teaching and research institutions in France or abroad, or from public or private research centers.

L'archive ouverte pluridisciplinaire **HAL**, est destinée au dépôt et à la diffusion de documents scientifiques de niveau recherche, publiés ou non, émanant des établissements d'enseignement et de recherche français ou étrangers, des laboratoires publics ou privés.

# Light-induced interconnects using nonlinear Airy beam interactions

**Bouchet T., Marsal N., Sciamanna M., Wolfersberger D.**

Chair in Photonics, LMOPS, CentraleSupélec, Université Paris-Saclay, F-57070 Metz, France

Chair in Photonics, LMOPS, CentraleSupélec, Université de Lorraine, F-57070 Metz, France

E-mail: [thomas.bouchet@centralesupelec.fr](mailto:thomas.bouchet@centralesupelec.fr)

**Abstract.** We analyze numerically optical waveguiding structures created in photorefractive media by two incoherent counter-propagating 1-D Airy beams under anti-symmetric nonlinear self-focusing conditions. We then inject a Gaussian probe beam to test our waveguiding structure. By using an anti-symmetric Airy beam configuration in stationary conditions, we find rich and complex waveguiding structures with multiple input to multiple output configurations and transverse input-to-output shifts up to 13 times the guided beam's waist.

## 1. Introduction

In 1979, in the context of quantum mechanics, Berry and Balazs predicted a new solution to the Schrödinger equation [1], the Airy wave packets. In 2007, by truncating the ideal Airy waveform the first optical Airy beam was observed in free space [2]. This self-healing, shape-preserving, accelerating beam has multiple applications from manipulating microparticles [3] and plasma channel generation [4] to all-optical routing [5], or light-sheet microscopy [6]. Recently, the self trapping character of Airy beams in biased nonlinear media has suggested interesting dynamics such as soliton-like behaviors [7, 8, 9, 10, 11]. Co-propagating Airy beams and their interactions have been studied in different medias ranging from nematic liquid crystals [12] to photonic lattices [13] or three-wave systems [14]. In Kerr or photorefractive media, the solitonic structures of two co-propagating coherent Airy beams will exhibit attraction when in-phase and repulsion when out-of-phase [15, 16, 17] whereas two incoherent Airy beams will always exhibit attraction [18]. Other research on the propagation dynamics have shown that by using external potentials and weakening or strengthening of the autofocussing effect, the accelerating trajectory of Airy beam like structures can be controlled [19, 20]. The interaction of Airy beams and solitons in nonlinear media can even reproduce gravitational dynamics [21].

Similarly to studies with two co-propagating Airy beams, two counter-propagating Airy beams in a saturable nonlinear media will shed off-shooting solitons given enough nonlinearity strength [22], furthermore the off-shooting solitons tend to be attracted by the lobes of the counter-propagating Airy beam [23]. However, by contrast to studies with two co-propagating Airy beams, a counter-propagating configuration combined with the large transverse dimension of the Airy shape and their curved trajectory allow several interaction schemes where one or several lobes of the counter-propagating beams can overlap [10, 22, 23]. The interaction of such counter-propagating Airy beams introduce new dynamics and open new interesting fields for optical interconnections. Interestingly, both multiplexing (combining light beams in a single waveguide) and demultiplexing (splitting light beams in different waveguides) can be achieved using Airy beams. Moreover, waveguiding with a greater output-to-input transverse shift can be obtained by using Airy beams rather than with conventional Gaussian beams.

Waveguiding possibilities in the case of counter-propagating Airy beams have been studied in a symmetric configuration [22], but to our knowledge no study exists on an anti-symmetric configuration.

In this letter we analyze numerically optical waveguiding structures created in photorefractive (PR) media by two incoherent counter-propagating 1-D Airy beams under nonlinear self-focusing conditions. In order to create complex waveguides we chose to propagate the Airy beams anti-symmetrically i.e. with each Airy beam accelerating towards the counter-propagating beams. This allows a larger overlapping of the Airy beams' secondary lobes. The overlapping results in stronger waveguiding structures with multiple input to multiple output configurations and transverse input-to-output

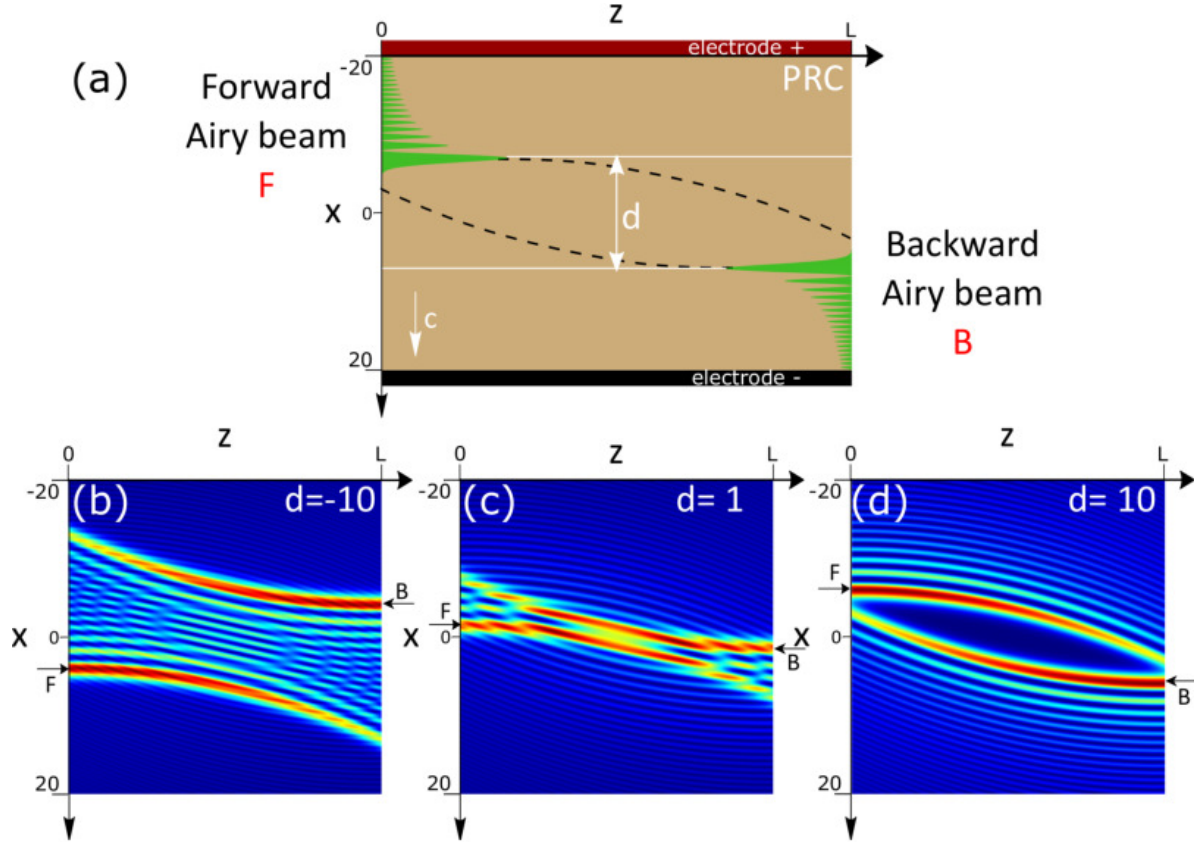


**Figure 1.** (a) Typical scheme of antisymmetric Airy beams' interaction in a PR crystal of length  $L$ . (b-c-d) Intensity distribution obtained for different values of shift  $d = -10, d = 1, d = 10$ . ( $F_0^2 = B_0^2 = 35$ ,  $x_0 = 10\mu m$ ,  $a = 0.03$ ,  $L = 3 = 1.63cm$ .)

shifts up to 13 times the guided beam's waist.

## 2. Antisymmetric Airy beams interactions scheme

The typical scheme of antisymmetric Airy beams is presented in figure 1(a). Both beams propagate in a PR crystal along the  $z$ -axis. The forward beam  $F$  propagates from left to right and the backward beam  $B$  propagates from right to left.  $d$  is defined as the shift along the  $x$ -axis between the forward and backward Airy beam's main lobes upon injection at each side of the crystal.  $L$  is the length of the PR crystal. The  $x$ -axis is normalized by  $x_0 = 10\mu m$  i.e. the Airy beams main lobe waist at  $1/e$  of its maximum intensity. The  $z$ -axis is normalized by the diffraction length  $L_d = 4\pi n_b x_0^2 / \lambda = 5.4mm$ , with  $n_b$  the unperturbed refractive index and  $\lambda$  the wavelength. The electric field is applied along the  $c$ -axis, parallel to the  $x$ -axis: this concerns nonlinear self-focusing conditions. The figure 1(b-c-d) show the intensity distribution of two counter-propagating anti-symmetrical Airy beams in linear conditions for different values of  $d$ . In a PR crystal due to the Pockels effect, the intensity distribution induces optically a refractive index distribution which can also be

seen as a waveguiding structure. In the case  $d = 1$ , the secondary lobes of the Airy beams greatly overlap resulting in a larger total intensity all along the secondary lobes' trajectory through the crystal and therefore corresponding to stronger variations of the refractive index. In what follows, we will mainly focus on this configuration which allows strong, numerous and complex waveguiding structures to appear.

The truncated Airy beams' input profiles are given by the following equations:

$$F(x, z = 0) = F_0 \text{Ai}\left(x + \frac{d}{2}\right) \exp\left(a\left(x + \frac{d}{2}\right)\right) \quad (1)$$

$$B(x, z = L) = B_0 \text{Ai}\left(-x - \frac{d}{2}\right) \exp\left(a\left(-x - \frac{d}{2}\right)\right) \quad (2)$$

where  $F_0$  (respectively  $B_0$ ) is the wave amplitude,  $\text{Ai}$  is the Airy function,  $a$  the truncation parameter of the Airy beam.

To simulate the behavior of the propagation of the antisymmetric Airy beams, we use the same theoretical model as in references [10, 11, 22, 23, 24]. The nonlinear propagation of the two incoherent counter-propagating beams can be expressed as follows:

$$i\partial_z F + \partial_x^2 F = \Gamma E_0 F \quad (3)$$

$$-i\partial_z B + \partial_x^2 B = \Gamma E_0 B \quad (4)$$

where  $\Gamma = (kn_b x_0)^2 r_{\text{eff}} E_e$  is the nonlinear photorefractive coupling strength,  $r_{\text{eff}}$  is the effective component of the electro-optic tensor and  $E_e$  is the external electric field.  $E_0$  is the homogeneous part of the x-component of the photorefractive space-charge field normalized by the external electric field. The temporal evolution of the space-charge field  $E_0$  is considered with a saturable nonlinearity and calculated using a relaxation-type dynamic:

$$\tau \partial_t E_0 + E_0 = -\frac{I}{1 + I} \quad (5)$$

where the relaxation time of the crystal  $\tau$  is inversely proportional to the total intensity  $\tau = \frac{\tau_0}{1+I}$ , and  $I = |F|^2 + |B|^2$  is the intensity normalized by the effective background intensity.

For small values of  $\Gamma$  ( $< 7$ ), the nonlinear effect is not high enough for producing waveguiding structures; when  $\Gamma > 15$  unstable dynamics are observed [22]. In this paper we present numerical simulations with a nonlinear photorefractive coupling strength  $\Gamma = 9$  which allows the analysis of rich and complex stable waveguiding structures

### 3. Optical interconnections for a transverse shift $d = 1$

In what follows, we focus on the configuration  $d = 1$  and  $\Gamma = 9$  because it has a rich variety of complex and interesting waveguiding structures. We are interested in the number of different outputs for a single input and in the transverse input-to-output shift of the waveguide.

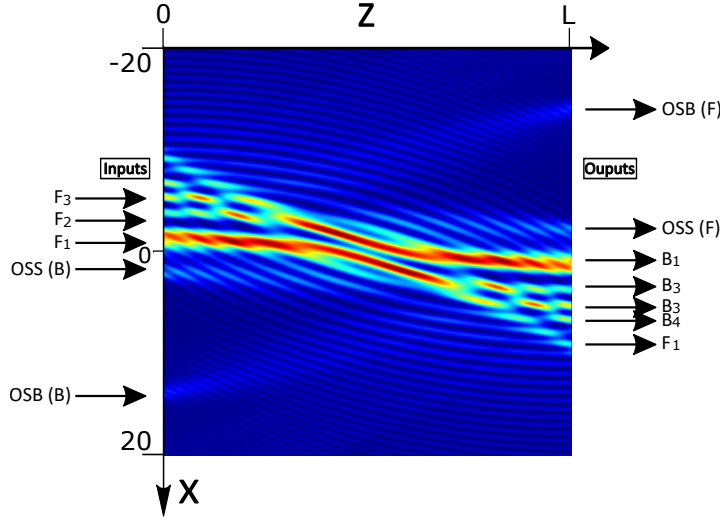


**Figure 2.** Intensity distribution of two counter-propagating anti-symmetrical Airy beams in non-linear self-focusing conditions with  $d = 1$ ,  $\Gamma = 9$ ,  $F_0^2 = B_0^2 = 35$ ,  $L = 3 = 1.63\text{cm}$ .

Figure 2 shows the intensity distribution of two counter-propagating anti-symmetrical Airy beams in non-linear self-focusing conditions for  $d = 1$  and  $\Gamma = 9$ . When the nonlinear self focusing effect compensates the diffractive nature of a light beam, a soliton-like structure appears [11]. The self focusing creates two new waveguiding structures of interest, an off-shooting beam (OSB) and an off-shooting soliton (OSS). The waveguiding structure shows different possible inputs, the OSB and OSS positions created by the backward Airy beam propagation,  $F_1$  the forward Airy beams main lobe position,  $F_2$  and  $F_3$  the forward Airy beams secondary lobes position respectively. The waveguiding structure also shows different possible outputs, the OSB position and OSS position created by the forward Airy beam  $F$ ,  $B_1$  the backward Airy beam's main lobe position,  $B_2$ ,  $B_3$  and  $B_4$  the backward Airy beam's secondary lobes positions respectively, and finally  $F_1$  the forward Airy beam's main lobe position after propagating through the crystal. The forward Airy beam's secondary lobes positions after propagating through the crystal are superimposed with the backward Airy beam's secondary lobe positions.

In order to analyze this waveguiding structure, we propagate a Gaussian probe beam (of waist  $x_0 = 10\mu\text{m}$ ) at different input positions of our crystal. The Gaussian probe beam's amplitude represents 10% of the Airy beam's amplitude in order for it's propagation to be linear. Figures 3(a-e) show the Gaussian beam's propagation in the waveguiding structure. The arrows at the left show the input probe beam's position and the arrows at the right show the output beam's positions. Figures 3(f-j) plot the corresponding amplitude and position of the input Gaussian beam (dotted line) and the resulting output beams transverse profile (solid line). It is worth mentioning that an output with less than 10% of the amplitude of the input beam is not of interest for

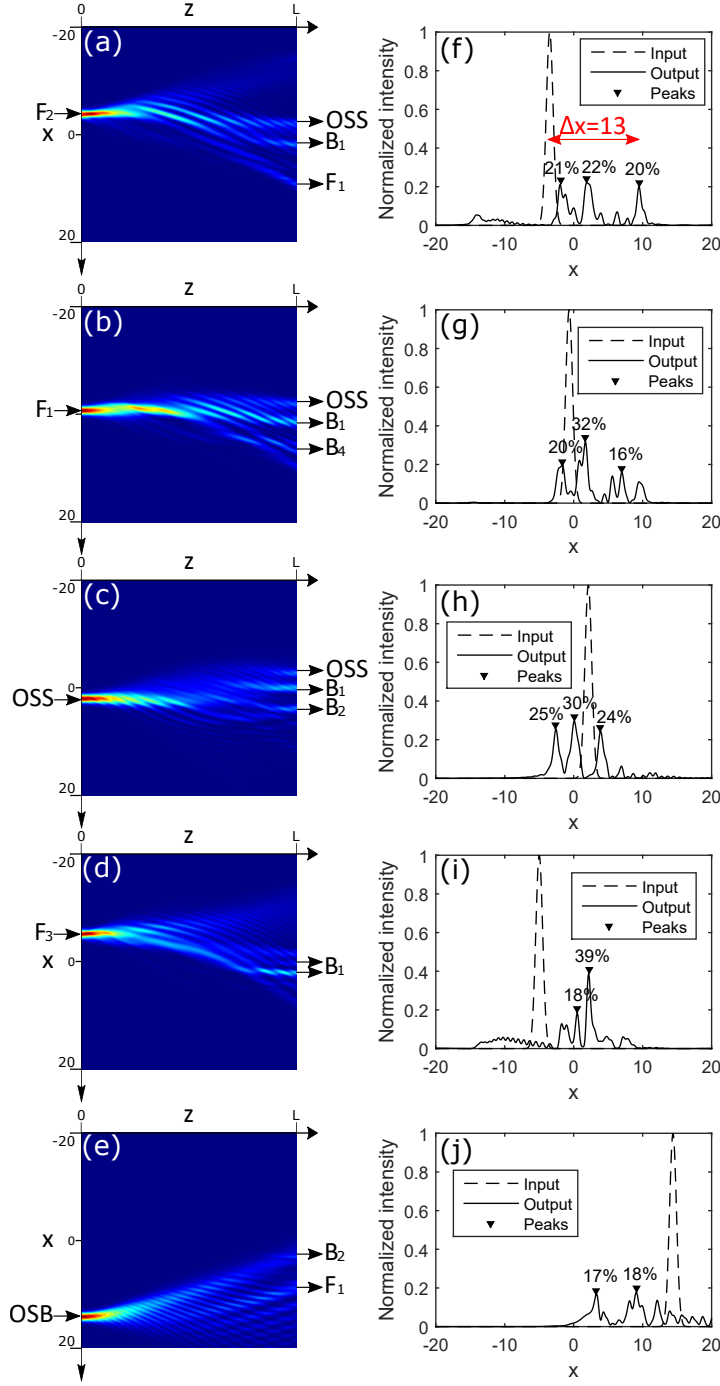


**Figure 3.** Linear probe beam propagation in the waveguide structure of figure 2 ( $d = 1$ ,  $\Gamma = 9$ ,  $F_0^2 = B_0^2 = 35$ ,  $L = 33 = 1.63\text{cm}$ .) (a-e) Intensity distribution. (f-j) Transverse intensity profiles of a Gaussian beam guided from different input positions ( $F_2$ ,  $F_1$ , OSS,  $F_3$ , OSB) respectively.

optical interconnects applications. We therefore decided to take into account only the output peaks that are over 15% of the input probe beam's maximum intensity. Some guiding behaviors were already predicted in previous studies of our group in the case of the symmetric Airy beam configuration [22]. By comparison, in this anti-symmetrical configuration, we observe a larger number of outputs for all cases. In figure 3(a), for a probe beam injected in  $F_2$  we observe simultaneously three outputs (OSS,  $B_1$  and  $F_1$ ) of equal peak intensity (around 20%). The OSS output is an expected output as it is observed even when the waveguide is obtained by injecting a single forward Airy beam [22]. However the two additional outputs called  $B_1$  and  $F_1$  are only obtained because of the interaction with the backward beam and thanks to the anti-symmetric configuration. For the symmetric counter-propagating beams interaction, the configuration with  $F_2$  as an input did not yield interesting waveguiding. Similarly in figures 3(b-c), injecting in  $F_1$  (respectively in the OSS) yields the expected OSS and  $B_1$  outputs but we also observe an additional  $B_4$  (respectively  $B_2$ ) output. Other inputs give interesting results:  $F_3$  and OSB [figure 3(d-e)]. We obtain for both cases two outputs, for the first case in the  $B_1$  area and for the second case in  $B_2$  and  $F_1$  positions. The fact that these inputs did not give any outputs in the previous study [22] shows the effectiveness of overlapping anti-symmetric secondary lobes.

The resulting photoinduced waveguiding structure yields more possibilities than what can be observed with counter-propagating Gaussian beams and even with Airy beams in a symmetrical configuration. The resulting waveguiding structure shows interesting features: we observe new optical interconnection schemes such as one input to three outputs with input-output shifts up to  $13x_0$  [figure 3(a)] (Shifts of only  $6x_0$  were observed for symmetrically counter-propagating Airy beams [22]).

During our investigation we also found other interesting waveguiding possibilities when the probe beam is not injected in one of the inputs mentioned in figure 2 but in between them. In doing so, other configurations are obtained by a coupling of evanescent waves at the different input positions and they are reported in figure 4. By injecting the probe beam between  $F_1$  and  $F_2$  [figure 4(a)] we combine outputs of the two cases presented in figure 3(a-b) ( $B_1$ ,  $B_4$  and  $F_1$ ) while suppressing others (OSS). Similarly by injecting between the OSS and  $F_1$  [figure 4(c)], we combine two outputs (OSS and  $B_2$ ) but lose two outputs ( $B_1$  and  $B_4$ ). In figure 4(b), by placing the probe beam at the top of guide  $F_1$  we can suppress the topmost output (OSS) while preserving the lobe outputs ( $B_1$  and  $B_4$ ). In figure 4(d) by placing the probe beam below the OSS input, we suppress the bottommost outputs ( $B_1$  and  $B_2$ ) and preserve the OSS output.

Such mechanics in Airy beam interactions can lead to the engineering of complex modular optical waveguides by varying different parameters such as the shift  $d$  between the beams, the nonlinearity of the medium and the size of the probe beam compared to the Airy beam .



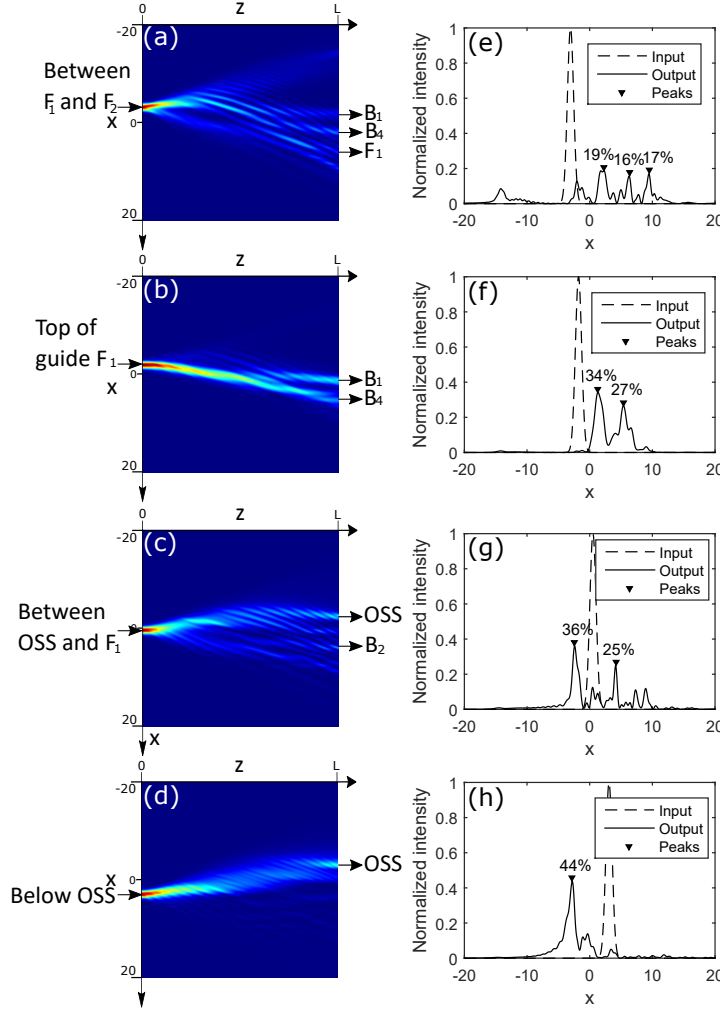


**Figure 4.** Linear probe beam propagation in the waveguide structure of figure 2 ( $d = 1$ ,  $\Gamma = 9$ ,  $F_0^2 = B_0^2 = 35$ ,  $L = 3$ )

#### 4. Stability of the photoinduced waveguide

In order to get an overall picture of the different waveguiding possibilities, we have plotted a mapping of the output intensity distribution versus  $x$  for different input probe beam positions (figure 5). For each input probe beam position, going from  $-20x_0$  to  $20x_0$ , we draw the output intensity distribution. If the output profile does not change for a certain range of input positions, we observe wide horizontal spots, showing a range of stability for the waveguide structure. If there are multiple outputs for a certain position of input we observe vertically multiple spots. The cases analyzed in figures 3 and 4 are reported in the mapping of figure 5(b). The most intense spots correspond to the best waveguiding conditions reported previously. The spots furthest from the topleft to downright diagonal (red) reveal the largest shifts from input to output positions. Circled in red is the  $F_1$  output for the  $F_2$  input [figure 3(a)] with an input to output shift equal to  $13x_0$ . Figures 5 (a) and (c) show the waveguiding behavior of counter-propagating

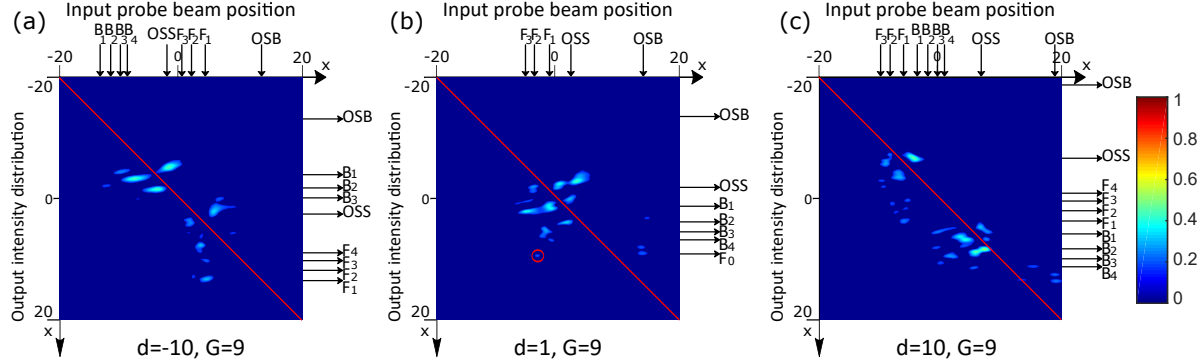


**Figure 5.** Intensity distribution of the probe beam at the output of the PR crystal for different input positions of the probe beam. ( $\Gamma = 9$ ,  $F_0^2 = B_0^2 = 35$ ,  $L = 3$ ). (a) Shift  $d = -10$ . (b) Shift  $d = 1$ . (c) Shift  $d = 10$ .

anti-symmetric Airy beams for  $d = -10$  and  $d = 10$  respectively. The configuration differs only by the shift  $d$  between the forward and backward Airy beams, but the resulting waveguiding behaviors are quite different. As expected, most spots are close to the diagonal because it corresponds to an input-to-output shift of 0 but multiple outputs are still observed. For example in the case  $d = -10$  [figure 5(a)], the probe beam injected in the OSS position has two output positions  $B_1$  and  $B_2$  which is the same result obtained for a single forward beam [22]. In the case  $d = 10$  however [figure 5(b)], the probe beam injected in the OSS position has three output positions  $F_1$ ,  $B_1$  and  $B_2$ . Therefore, figure 5 summarizes how changing parameters like the transverse shift  $d$  between forward and backward beam or the nonlinearity of the medium can give new waveguiding possibilities in comparison to the situation of photoinduced waveguiding from a single Airy beam or even two symmetric counter-propagating Airy beam.

## 5. Conclusion

We have analyzed the waveguides photoinduced by two counter-propagating anti-symmetric Airy beams. We have analyzed the propagation behavior of a Gaussian probe beam in such waveguides. We have found configurations giving multiple outputs for multiple input positions: up to three outputs whereas previous works had up to two outputs [22]. We have found greater input-to-output shifts (up to 13 beam waists) with counter-propagating anti-symmetric Airy beams compared to what was possible with counter-propagating Gaussian beams or even counter-propagating symmetric Airy beams configuration (typically maximum 6 beam waists [22]). Interactions of Airy beams in nonlinear self-focusing conditions yield much broader all-optical waveguiding possibilities than those observed so far with Gaussian beams. The situation discussed

here with so-called anti-symmetric counter-propagating Airy beams yields to our knowledge the largest variety of all-optical waveguiding: either single input to single output but with possibly large transverse shifts, either single (multiple) inputs to multiple (single) outputs just by varying the initial transverse shift between the counter-propagating Airy beams or the nonlinearity strength.

## Acknowledgments

We acknowledge the support of AIRBUS-GDI Simulation, Metz Métropole, Conseil Départemental de Moselle, Conseil Régional Grand-Est, Préfecture de Région Grand-Est, FEDER, CentraleSupélec, Fondation Supélec through the funding of the Chair in Photonics.

## References

- [1] Michael V Berry and Nandor L Balazs. Nonspreading wave packets. *Am. J. Phys.*, 47(3):264–267, 1979.
- [2] Georgios A Siviloglou and Demetrios N Christodoulides. Accelerating finite energy airy beams. *Opt. Lett.*, 32(8):979–981, 2007.
- [3] Jörg Baumgartl, Michael Mazilu, and Kishan Dholakia. Optically mediated particle clearing using airy wavepackets. *Nat. Photonics*, 2(11):675–678, 2008.
- [4] Pavel Polynkin, Miroslav Kolesik, Jerome V Moloney, Georgios A Siviloglou, and Demetrios N Christodoulides. Curved plasma channel generation using ultraintense airy beams. *Science*, 324(5924):229–232, 2009.
- [5] Patrick Rose, Falko Diebel, Martin Boguslawski, and Cornelia Denz. Airy beam induced optical routing. *Appl. Phys. Lett.*, 102(10):101101, 2013.
- [6] Tom Vettenburg, Heather IC Dalgarno, Jonathan Nylk, Clara Coll-Lladó, David EK Ferrier, Tomáš Čižmár, Frank J Gunn-Moore, and Kishan Dholakia. Light-sheet microscopy using an airy beam. *Nat. Methods*, 11(5):541–544, 2014.
- [7] Ido Kamimer, Mordechai Segev, and Demetrios N Christodoulides. Self-accelerating self-trapped optical beams. *Phys. Rev. Lett.*, 106(21):213903, 2011.
- [8] Falko Diebel, Bojana M Bokić, Dejan V Timotijević, Dragana M Jović Savić, and Cornelia Denz. Soliton formation by decelerating interacting airy beams. *Optics Express*, 23(19):24351–24361, 2015.
- [9] Ming Shen, Jinsong Gao, and Lijuan Ge. Solitons shedding from airy beams and bound states of breathing airy solitons in nonlocal nonlinear media. *Scientific reports*, 5:9814, 2015.
- [10] Noémi Wiersma, Nicolas Marsal, Marc Sciamanna, and Delphine Wolfersberger. Airy beam self-focusing in a photorefractive medium. *Sci. Rep.*, 6:35078, 2016.
- [11] Thomas Bouchet, Nicolas Marsal, Marc Sciamanna, and Delphine Wolfersberger. Solitonic characteristics of airy beam nonlinear propagation. *Physical Review A*, 97(5):051801, 2018.
- [12] Ming Shen, Wei Li, and Ray-Kuang Lee. Control on the anomalous interactions of airy beams in nematic liquid crystals. *Optics express*, 24(8):8501–8511, 2016.
- [13] Zhiwei Shi, Jing Xue, Xing Zhu, Ying Xiang, and Huagang Li. Interaction of airy-gaussian beams in photonic lattices with defects. *Physical Review E*, 95(4):042209, 2017.
- [14] Thawatchai Mayteevarunyoo and Boris A Malomed. The interaction of airy waves and solitons in a three-wave system. *Journal of Optics*, 19(8):085501, 2017.
- [15] Yiqi Zhang, Milivoj Belić, Zhenkun Wu, Huaibin Zheng, Keqing Lu, Yuanyuan Li, and Yanpeng Zhang. Soliton pair generation in the interactions of airy and nonlinear accelerating beams. *Opt. Lett.*, 38(22):4585–4588, 2013.

- [16] Yiqi Zhang, Milivoj R Belić, Huaibin Zheng, Haixia Chen, Changbiao Li, Yuanyuan Li, and Yanpeng Zhang. Interactions of airy beams, nonlinear accelerating beams, and induced solitons in kerr and saturable nonlinear media. *Optics express*, 22(6):7160–7171, 2014.
- [17] Meizhi Zhang, Guangwen Huo, Hua Zhong, and Zhanqiang Hui. Interactions between self-accelerating beams in photorefractive media. *Optics express*, 25(18):22104–22112, 2017.
- [18] Ming Shen, Liang Wu, Mingming Gao, and Wei Li. Incoherent interactions of airy beams in nonlocal nonlinear media. *Journal of Physics B: Atomic, Molecular and Optical Physics*, 51(16):165401, 2018.
- [19] Hua Zhong, Yiqi Zhang, Milivoj R Belić, Changbiao Li, Feng Wen, Zhaoyang Zhang, and Yanpeng Zhang. Controllable circular airy beams via dynamic linear potential. *Optics express*, 24(7):7495–7506, 2016.
- [20] Yiqi Zhang, Milivoj R Beli, Lei Zhang, Weiping Zhong, Dayu Zhu, Ruimin Wang, and Yanpeng Zhang. Periodic inversion and phase transition of finite energy airy beams in a medium with parabolic potential. *Optics express*, 23:10467–10480, April 2015.
- [21] Rivka Bekenstein, Ran Schley, Maor Mutzafi, Carmel Rotschild, and Mordechai Segev. Optical simulations of gravitational effects in the newton–schrodinger system. *Nature Physics*, 11(10):nphys3451, 2015.
- [22] Noémi Wiersma, Nicolas Marsal, Marc Sciamanna, and Delphine Wolfersberger. All-optical interconnects using airy beams. *Opt. Lett.*, 39(20):5997–6000, 2014.
- [23] Noémi Wiersma, Nicolas Marsal, Marc Sciamanna, and Delphine Wolfersberger. Spatiotemporal dynamics of counterpropagating airy beams. *Sci. Rep.*, 5:13463, 2015.
- [24] M Belić, Ph Jander, K Motzek, A Desyatnikov, D Jović, A Strinić, M Petrović, C Denz, and F Kaiser. Counterpropagating self-trapped beams in photorefractive crystals. *J. Opt. B: Quantum Semiclassical Opt.*, 6(5):S190, 2004.